Materials Today Communications 26 (2021) 101749

Contents lists available at ScienceDirect

Materials Today Communications

journal homepage: www.elsevier.com/locate/mtcomm

Dispersion of thulium-yttria nanoparticles to build up smart structures

S.C. Santos *, O. Rodrigues Jr, L.L Campos

Instituto de Pesquisas Energeticas e Nucleares – IPEN, Av. Prof. Lineu Prestes 2242, Cidade Universitaria, Sao Paulo, Brazil

ARTICLE INFO

Keywords:
Yttria
Thulium oxide
Rare earths
Lanthanides
Zeta potential
Ceramic processing

ABSTRACT

The development of new materials for radiation dosimetry is a challenge to assure quality improvement practices related to radiation protection concept. On this context, colloidal stability provides conditions to build up smart structured materials from bottom-up perspective. The present work reports zeta potential characterization of thulium-yttria nanoparticles in aqueous medium. Thulium-yttria nanoparticles formed by a relative low temperature hydrotermal synthesis were characterized by XRD, PCS, and SEM. The stability of particles in aqueous medium was evaluated by electrophoretic mobility measurements, followed by zeta potential calculation. The results revealed that the isoelectric point of thulium-yttria suspensions shifted in accordance with thulium concentration from pH 8.5 ("pure" yttria) to pH 9.2 (2at.%Tm). Besides, most suspensions could be stabilized at pH 10.5, presenting zeta potential values around 30 mV. These results are substantial parameters to advance toward new materials for radiation dosimetry.

1. Introduction

The research for new materials for radiation dosimetry is a key issue, which aims to improve quality-safety of all procedures in which ionizing radition is used [1]. Rare earth (RE) oxides are promising materials to enhance the protection of humans against the detrimental effects of ionizing radiation.

Yttria which synonym is yttrium oxide (Y_2O_3) is one of the most important RE sesquioxides due to mechanical, thermal and spectroscopic properties, covering a wide range of applications as, biomaterials [2], gas burners [3], sintering aids [4], membranes [5], catalysts [6], capacitors [7], thermal coatings [8], structural reinforcement [9], and luminescent devices [10]. Moreover, yttria exhibits as crystalographic characteristics cubic C-type structure at environmetal pressure, two points of symmetry (S_6, C_{3i}) and C_2, and large vacancies of Y and O [11–13]. For instance, these vacancies enable the insertion of additional rare earth elements into its lattice. Thus, yttria is addressed as host material for other RE ions such as Nd [14], Ce [15], Er [16], and Yb [17].

The remarkable effect of thulium (Tm) as activator of ceramic/glasses have been reported [18–22]. The purpouse of using thulium as activator of yttria consistis in the fact that the electronic levels of thulium ions can interact with energy leves of yttria, enhancing yttria characteristics for radiation dosimetry. Santos et al. [21] reported that dosimetric characteristics of yttria were remarlably improved by doping with 2at.% Eu (at.%, atomic percentage). The results revealed that samples exhibited electron paramagnetic response with linear behaviour during a dose range from 0.001 up to 50kGy.

In ceramic processing based on colloidal suspensions, the control of interparticle interactions is essential to produce ceramic materials and components with suitable properties. Stable suspensions usually provide dense powder compacts after shaping, and homogeneous microstructure as sintered. On the other hand, instable suspensions provide bodies with heterogeneities as cracks, surface inconsistences, asymmetries, and undesired microstructure. Therefore, the final properties of ceramic body rely on particle stability. This stability can be evaluated by measuring electrophoretic mobility of particles (μ_e), followed by zeta potential (ζ) calculation.

There are few works on colloidal dispersion of rare earth based materials. Recently our group reported a complete study on colloidal processing of yttria particles to produce ceramic nettings for gas lighting [23], as well as a review on colloidal processing of rare earths [24]. Besides, an approach to form yttria and europium-yttria micro rods by bio-prototyping were reported [25,26]. Therefore, there is a wide field for investigation on colloidal stability of yttria based nanoparticles.

This work reports a study on stability of thulium-yttria nanoparticles in aqueous medium, by measurements of electrophoretic mobility of particles, followed by zeta potential calculation. These stability parameters will be subsidies to advance toward new dosimetric materials based on thulium-yttria nanoparticles.

* Corresponding author.
E-mail address: silas.cardoso@alumni.usp.br (S.C. Santos).

https://doi.org/10.1016/j.mtcomm.2020.101749
Received 22 April 2020; Received in revised form 25 September 2020; Accepted 3 October 2020
Available online 10 October 2020

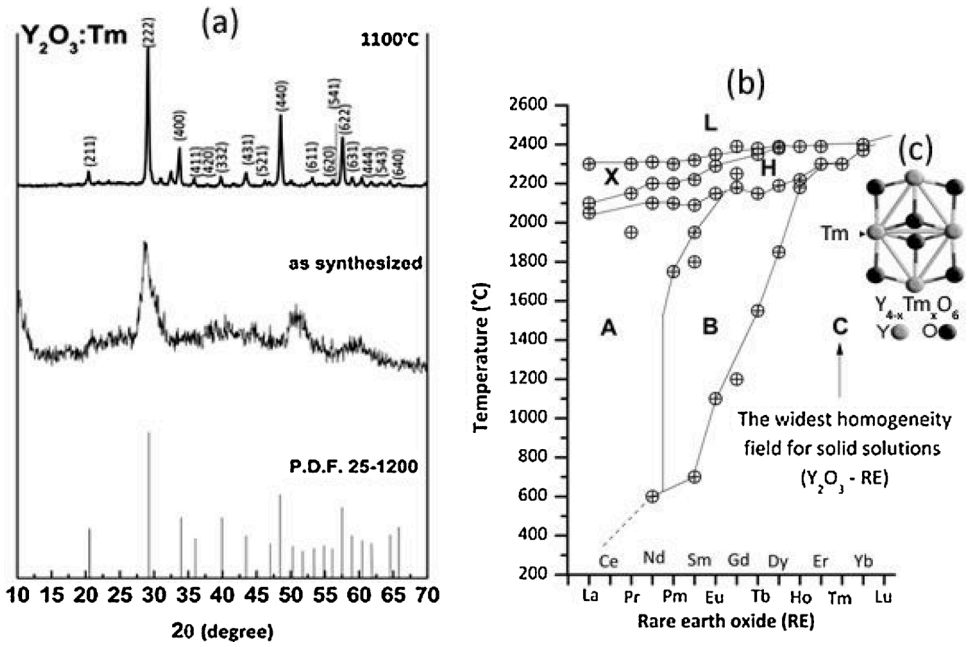

Fig. 1. (a) XRD curves of thulium-yttria powders formed by hydrothermal synthesis, and followed by thermal treatment at 1000 °C for 2 h in room atmosphere; (b) Phase formation diagram of the main rare earth oxides as a function of temperature; and (c) illustration of a crystal cluster from cubic C-type lattice – dark spheres mean oxygen (O) atoms, gray spheres yttrium (Y) atoms and the light sphere means Tm atom (dopant).

2. materials and methods

Cubic C-type thulium-yttria powders (Tm:Y_2O_3) were used as starting material. Stoichiometry synthesis of Tm:Y_2O_3 powders with up to 2at%.Tm (atomic percentage) was performed by hydrothermal process, in which a precursor gel was stirred at 60 °C for 6 h into a condenser system in order to keep the volume of suspension constant. The as synthesized powders were thermall treated at 1100 °C for 2 h, in air atmosphere in order to form crystalline samples (Lindberg Blue, Haake). The great advantage of this method consists in producing nanoparticles with controlled characteristics as size, shape, and stoichiometric composition, and using environmental pressure. Details on hydrothermal method used is reported in our recent work [27].

As synthesized Tm:Y_2O_3 powders were characterized by X-ray diffraction (XRD, Rigaku Multiflex, Japan), with an angular range (2θ) from 15 to 70°, scanning of 0.5°. min^{-1} and Kα source, in which crystallite size was calculate from Scherrer formula Eq.(1) [28], and based on the measurement of full-width at half-maximum (FWHM) values in the corresponding XRD pattern; Photon Correlation Spectroscopy (PCS, Litesizer500, Anton Paar), in which mean diameter (d_{50}) was calculated according to Eq.(2) [29]; helium pycnometric (Pycnometer Micrometrics 1330) to evaluate real density; Scanning Electron Microscopy (SEM, TM3000, Hitachi) to observe particle morphology and size; and stability of particles in aqueous medium by electrophoretic mobility measurements (μ_e) in room temperature (20 °C), followed by zeta potential calculation (ζ) based on Smoluchowski limit Eq.(3) [30,31]. To perform stability evaluation stock suspensions with 0.5 g L^{-1} of solids, 1 mM NaCl (58.54 g.Mol^{-1}, Merck) as indifferent electrolyte (which constituents are not electroactive on the range of applied potentials) [32], and HCl and KOH solutions were used.

$$d_c = \left(\frac{0.9\lambda}{\beta cos\theta}\right) [\text{nm}] \quad (1)$$

$$d_{50} = \left(\frac{K_{BT}}{3\pi\eta(T)D_t}\right)[nm] \quad (2)$$

Where, K_{BT} is Boltzmann constant (1.38064852.10^{-23} m^2. kg. s^{-2}. K^{-1}), T is temperature (K), η(T) is viscosity of the suspending liquid and, D_t is particle diffusion coefficient.

$$\zeta = \left(\frac{\mu_e.\eta}{\varepsilon}\right)[mV] \quad (3)$$

Where ε is permittivity of liquid ($J.V^{-2}$ m); η is the viscosity of liquid (cP); μ_e is the electrophoretic mobility of particles ($\mu.s^{-1}.V^{-1}cm$).

3. Results and discussion

Ceramic processing consists in a set of procedures in which powder manipulation is predominant. In addition, powder characteristics influence directly on further processing steps. As yttria exhibits lattice features that enable doping it with other rare earth ions as thulium (Tm^{3+}), new materials with improved characteristics can be produced. Y_2O_3 and Tm_2O_3 exhibits the same crystal lattice and quite similar atomic radius 1.80 Å and 1.75 Å, respectively [33]. Doping Y_2O_3 with Tm^{3+} provides substitution of Y^{3+} by Tm^{3+} in C_2 and S_6 sites with no significant distortion of crystal lattice.

XRD curves of thulium-yttria powders hydrothermally synthesized are illustrated in Fig.1a. As synthesized powders exhibited amorphous structure, in which a short range peak was recorded around 30° (2θ). On the other hand, samples treated at 1100 °C for 2 h presented cubic C-type structure, with three high intensity peaks recorded at 30.0° (222); 48.6° (440); 58.1° (622), and corresponding to Powder Diffraction File (PDF. 25–101). As reported in our recent investigations [24,25], crystalline yttria powders were formed using thermal treatment over 800 °C, in which uniform and crystalline particles were obtained around 1000−1100 °C. Moreover, Tolstikova et al. [34] and Lojpur et al. [35] reported that the thermal treatment at 1100 °C for 2 h provided crystalline particles of neodymium-yttria and ytterbium/erbium-yttria, respectively.

Rare earth sesquioxides (RE_2O_3) can present one of the following forms, A, B, C, X, and H, as shown in Fig. 1b. The C-type form presents cubic lattice, being the most favourable structure to be formed under environmental pressure and is stable at high temperature. For instance, from Er to Lu C-type form is stable over 2000 °C. The A-type presents hexagonal structure, whereas B-type is monoclinic. Just below the melting point the last two high temperature forms are situated. X-type

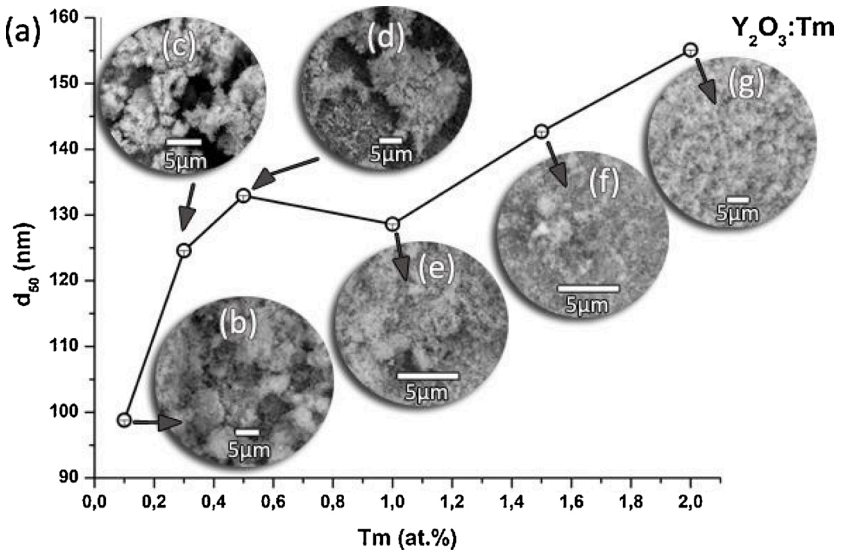

Fig. 2. Particle size and morphology of thulium-yttria nanoparticles with up to 2at.%Tm treated at 1100 °C for 2 h: (a) mean particle size; (b-g) SEM images.

presents hexagonal structure, while H-type is cubic. However, polymorphism of sesquioxides (including Y and Sc) have been reported under high pressure and temperature [36–38].

The incorporation of thulium ions into yttria lattice provides light rearrangement of yttria structure, seeing that Tm and Y presents similar ionic radius 175 pm and 180 pm, respectively [33]. Therefore, the process of Tm^{3+} incorporation is characteristically substitutive, as a result none secondary phase peaks were observed (Fig.1a). Tm^{3+} ion replaces Y ion in C_2 and S_6 sites with no significant distortion of crystal lattice as shown in Fig.1c.

Particle size and shape of thulium-ytrria powders with up to 2at.% Tm treated at 1100 °C for 2 h are illustrated in Fig. 2. The hydrothermal method provided ceramic particles in nano sized range (Fig.1a), in which the mean diameter (d_{50}) exhibited slight increase as a function of thulium concentration from 97 nm for 0.1at%Tm up to 156 nm for 2at% Tm. For crystallite size (d_c) no quite significant changes were observed.

As listed in Tab. 1, all samples presented moderate polydispersity distribution, seeing that polydispersity index (PDI) was less than 0.27, span (S, d_{90}-d_{10}) was inferior than 200 nm, as well as relative span (RS, S/d_{50}) is less than 2.0. As much as RS value is near to 1.0 (unity), it means that the particle size distribution is near to the unitary particle. Considering that thulium (Tm) presents almost twice the molar mass of yttrium (Y) 168.9 $g.Mol^{-1}$ and 88.91 $g.Mol^{-1}$ respectively, its incorporation into yttria lattice provided increase in pycnometric density from 4.94 $g.cm^{-3}$ up to 5.81 $g.cm^{-3}$. In our previous studies nanoparticles with mono modal distribution were prepared as, ß-yttrium disilicate [38] (ß-$Y_2Si_2O_7$) with d_{50} of 185 nm, ß-dysprosium doped yttrium disilicate [39] (ß-$Y_2Si_2O_7$:Dy) with d_{50} of 242 nm, and cubic C-type europium doped yttria [25] (Y_2O_3:Eu) with d_{50} of 576 nm.

As shown in Fig. 2b, all powder compositions (from b to g) presented the same morphology, consisting in agglomerates of rounded particles. Particles in nano sized range provide substantial conditions to innovate toward new materials for radiation dosimetry, once formation of the material begins from bottom-up scale. By suitable dispersion of nanoparticles dense compacts can be formed during shaping process, seeing that nanosized and uniform particulates enable high packed particles. Besides, after thermal treatment dense compacts usually exhibit controlled shape and size, dense microstructure (without detrimental defects), and suitable mechanical strength. Based on this concept, our group reported some studies on colloidal processing of rare earths in which ceramic components with controlled characteristics as shape, size and microstructure were formed as ß-yttrium disilicate [38] and ß-$Y_2Si_2O_7$:Dy [39] biomorphic burners, and Y_2O_3 nettings for gas lighting [22], and Y_2O_3:Eu micro rods [25] for radiation dosimetry.

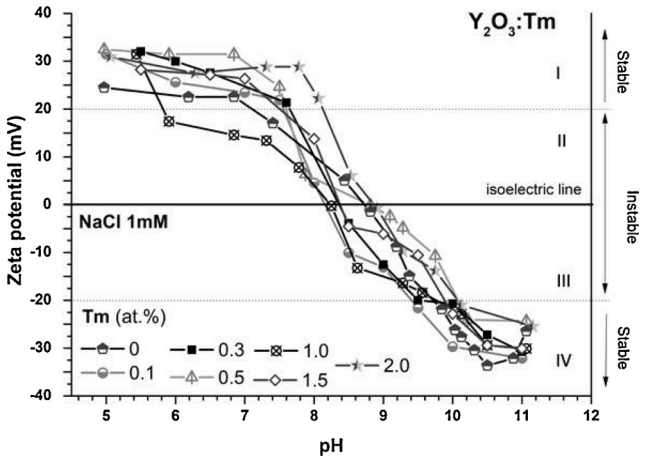

Fig. 3. Zeta potential curves of thulium-yttria suspensions as a function of pH.

During processing ceramic powders are under distinct procedures as mixing, comminution, and filtration in order to adequate their surface characteristics for further processing steps. Shaping processes from ceramic powders are usually performed by suspensions, and their flow behavior relies on particle characteristics, liquid medium in which they are immersed, and the interface between them.

In Fig. 3 are illustrated zeta potential curves of thulium-yttria suspensions prepared with 0.05 vol% particles, and 1 mM NaCl. The instability range for yttria suspensions, which means that ζ is inferior than |20 mV|, was from pH 7.1–9.7 - stages II and III. These stages represent the predominance of attraction forces in which weak and strong flocculated states take place, as illustrated in Fig. 3. In the weak flocculation state, particles form flocs in suspension at volume fractions below the gel point ($\Phi < \Phi_{gel}$) or a particle network at higher volume fractions ($\Phi \geq \Phi_{gel}$) with at least a minimum equilibrium separation (secondary minimum). On the other hand, in strong flocculation state particles form a particulate network, or individual clusters (primary minimum) [40]. Even that yttria exhibited significant zeta potential values in acid pH range it was not considered (stage I), seeing that in pH range below 5.5 rare earths present solubility as reported previously by Sprycha et al. [41]. High stability was observed at pH 10.5 with ζ of -34.56 mV (stage IV), being in agreement with our recent investigation

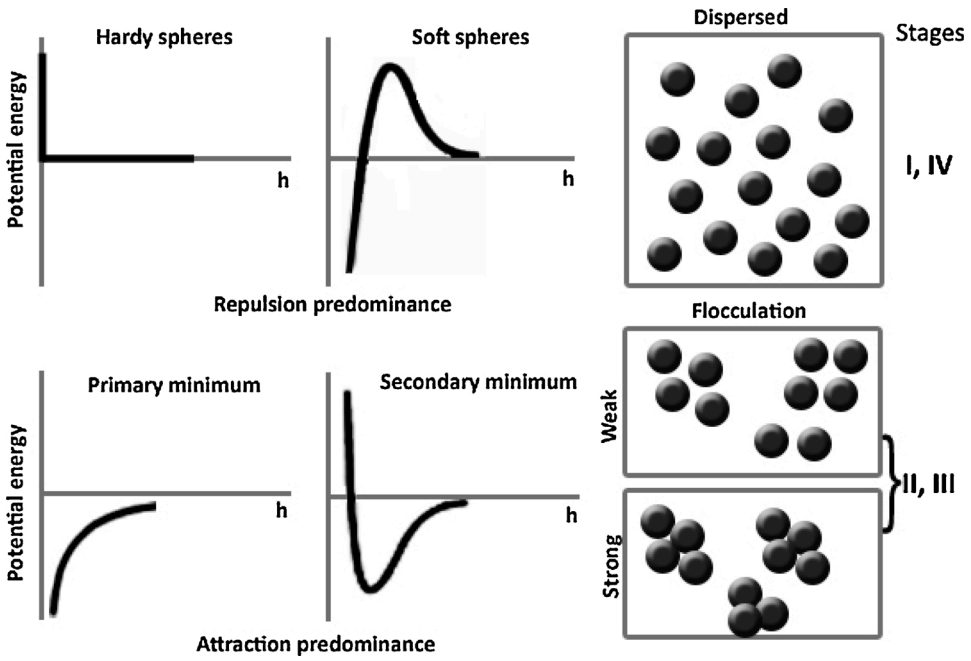

Fig. 4. Relationship between the total interparticle potential energy and the final suspension structure, illustrating the following modes: dispersed (I, IV), flocculated (II, III). Adapted from Lewis et al. [40].

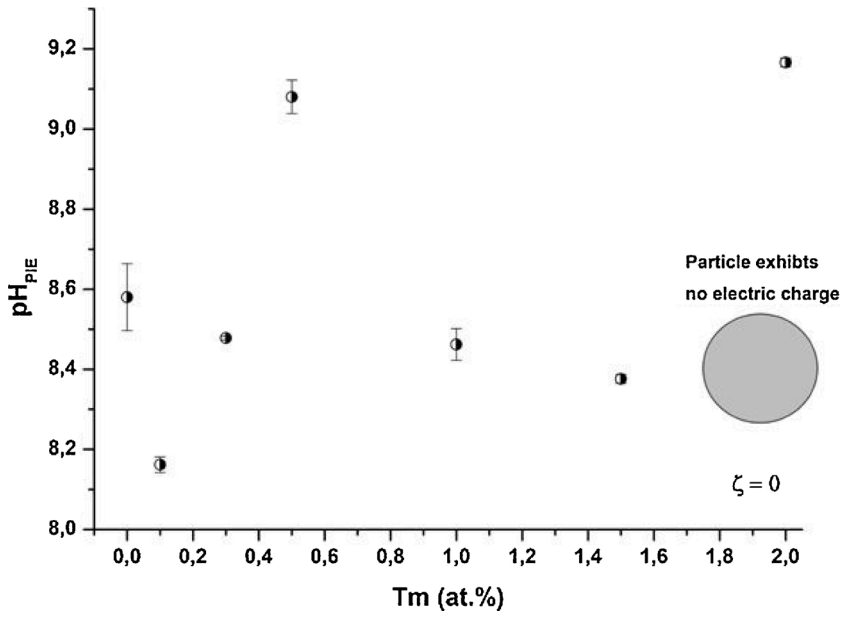

Fig. 5. Isoeletric point of thulium-yttria suspensions as a function of Tm concentration.

[22] on yttria nanoparticles with d_{50} 131.8 nm.

Colloidal stability is governed by a sum of interparticle potential energies (V_c) which comprehends the following potential energies: van der Waals interactions (V_W), repulsive from electrostatic interactions (V_e), repulsive from steric interactions (V_s), structural interactions from non adsorbed species in solution that can increase or decrease suspension stability (V_t). Therefore, to stabilize colloidal suspensions (Fig. 4, stages I and IV) the conditions of liquid medium in which they will be immersed should be adjusted in order to provide high repulsive interparticle interactions in detrimental of those attractive ones.

Doping yttria with thulium was effective on shifting IEP of yttria from pH 9.2 ("pure yttria") to pH 8.5 (2at.%Tm), as illustrated in Fig.3. The advantage of shifting IEP is to make larger the pH range in which particles become stabilized. Considering that stable suspensions can be prepared by setting pH far from IEP, the results reveal that most of thulium-yttria compositions can be stabilized at pH around 10.5–11.0 (stage IV). In contrast, thulium-yttria compositions with 0.5 and 2.0at.% Tm presented high zeta potential values near to central pH scale (7) as pH 6.8 and pH 7.3, respectively. Besides, these two compositions presented similar zeta potential curves, including quite similar IEP as 9.1 and 9.2.

For thulium-yttria suspensions is observed a slight displacement of IEP according to thulium concentration from pH 8.6 to pH 9.2, as illustrated in Fig.5. "'Pure" yttria (Tm 0at%) exhibited isoelectric point (IEP) at pH 8.6 [39,40] When the pH of suspension is set at IEP the number of positive ions become equivalent with the number of negative

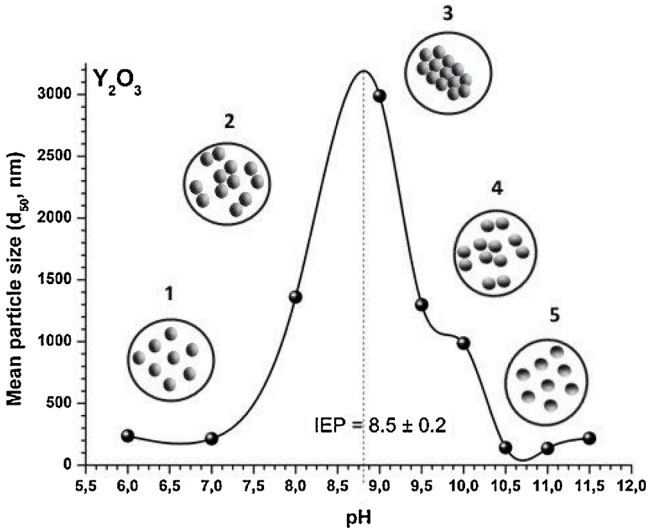

Fig. 6. Effecf of pH on promotion of the mean particle size and dispersion state of yttria powders: (1,5) dispersed; (2,4) weak flocculated; and (3) strong flocculated.

ions, thus this ion equivalence provides destruction of electric double layer and particles become unstable. Besides, zeta potential (ζ) value becomes 0 and attraction forces are predominant. As a consequence, particles begin to flocculate and sediment. Moreover, adding additives into suspension to improve particle dispersion (silicates, phosphates, and anionic polyelectrolytes) provides displacement of the IEP toward acid pH range. In our work [23] on yttria nanoparticles, using 1.0 wt.% (weight percentage) poly-acrylic acid (PAA) as dispersant provided displacement of IEP from pH 8.5 to pH 6.4. Furthermore, stable suspensions could be prepared apart from pH 7 using 0.5 wt%PAA. Angel-Olarte et al. [41] reported that aqueous co-doped gadolinium suspensions (Gd_2O_3:Eu^{3+}/Yb^{3+}) exhibited IEP at pH 7.7, being stable at pH 9.5 (ζ >20 mV).

Colloidal processing is not exclusively based on dispersion of particles. Sometimes the procedure of flocculation is performed in order to separate at least two different phases. Liu et al. [42] reported a study on pre-treatment and filter configuration for removing surrogates of Cryptosporidium oocysts in cold-water conditions, in which zeta potential was performed in order to evaluate water filtration process. Moreover, our research group reported studies on colloidal stability of rare earths in which porous, reticulated, and biomorphic structures of rare earth based materials such as Y_2O_3 [43], RE_2O_3 [44], $Y_2Si_2O_7$ [45], and $Y_2Si_2O_7$:Dy [46] were produced.

Zeta potential relies on charge density of the electric double layer formed on particles, which in turn depends on conditions of the medium wherein they are immersed. In aqueous medium the pH is a key parameter that provides substantial conditions to both disperse, and agglomerate particles. As Y_2O_3 particles are immersed in aqueous medium, the hydration of their surface could induce the formation of new chemical species. The surface oxygen can be hydrolyzed constituting rare earth metal-hydroxide groups, as shown in eq. 4.

$$YO + [OH^- + H^+] \leftrightarrow YOH + OH \quad (4)$$

In Fig. 6 is illustrated the effect of pH on dispersion of yttria particles. As reported previously, yttria presents IEP at pH 8.5, which means that only attraction forces are predominant and promote the formation of flocs or cluster of particles. As a result, at pH 9 the mean particle size (d_{50}) was 2988.4 nm, a value extremely elevated. On the other hand, setting pH far from IEP provides significant reduction on d_{50}, which means that repulsion forces are intensified in detriment of attraction ones. For instance, d_{50} decreased from 2988.4 nm at pH 9 (near to IEP) to 213.9 nm at pH 7 and to 135 nm to pH 11, respectively. At pH 11.5 formation of particle agglomerates is observed, in which d_{50} was 216.8 nm. This result is in accordance with those reported on zeta potential curves (Fig. 3). Apart from pH 10.5 the thicknesses of the electric double layer begins to decrease due to increase of ionic strength, and as a consequence, ζ values decrease.

The insertion of thulium into yttria lattice did not provide remarkable changes on particle characteristics such as size, shape, and crystal structure, seeing that rare earth oxides exhibit great similarity of chemical and physical properties. However, a significant change on surface chemistry of particles characterized by zeta potential in aqueous medium was observed.

The effect of activator on yttria is often observed by additional characterizations. Nevertheless, it is beyond the scope of this paper. According to our previous work, doping yttria with 2at.% europium (atomic percentage, at.%) led to improvement of Electron Paramagnetic Resonance (EPR) response of ceramic rods, in which samples exhibited a great increase of dose sensitiveness in dose range from 0.001 up to 10kGy [26]. This effect is based on a set of features as phase stability, increase of luminescence centres, and higher probability of radiative recombination [47,48]. In addition, Govimdasamy et al. [11] reported that RE-doped yttria exhibits higher luminescence response due to RE ions are located at C_2 sites of yttria (Table 1).

Considering that rare earth oxides present unique properties and are quite expensive materials, many efforts have been proposed in order to use these substances in sustainable manner. Based on this concept the present work innovates by evaluating and reporting the stability parameters for colloidal processing in aqueous medium of these valuable materials, as listed in Table 2. The establishment of stability conditions provides very useful parameters to advance toward new materials for radiation dosimetry.

Table 1
Characteristics of Y_2O_3:Tm particles obtained by hydrothermal synthesis.

Tm (at.%)	Particle size distribution (nm)						ρ (g. cm^{-3})
	d_{10}	d_{50}	d_{90}	d_c	S	RS	
0	81.9	135.8	215.8	117	133.9	0.99	4.94
0.1	75.8	98.8	135.7	4.7	59.9	0.61	4.99
0.3	64.9	124.6	185.0	6.2	120.1	0.96	5.18
0.5	70.0	132.9	184.2	6.9	114.2	0.86	5.25
1.0	74.7	128.6	240.2	6.6	165.5	1.29	5.45
1.5	117.0	142.7	264.7	5.5	147.7	1.04	5.52
2.0	104.9	155.1	317.0	5.1	212.1	1.37	5.81

at.%: atomic percentage; S (Span): d_{90}-d_{10}; d_c: crystallite size; RS (Relative Span): Span/d_{50}; ρ: pycnometric density.

Table 2
Stability parameters for thulium-yttria suspensions.

Tm (at.%)	High dispersion		Instable range	IEP
	pH	ζ (mv)	pH	
0	10.5	−34.56	7.1 – 9.7	8.5
0.1	10.0	−31,03	7.5 – 9.4	8.2
0.3	11.0	−32.13	7.6 – 10.0	8.5
0.5	6.8	31.38	7.6–10	9.1
1.0	10.5	−30.37	5.8 – 9.9	8.5
1.5	10.5	−29.93	7.6 – 9.9	8.4
2.0	7.3	28.73	8.1 – 10.1	9.2

at.%: atomic percentage; Instable range means $|\zeta| < 20$ mV.

4. Conclusion

The stability of cubic C-type thulium-yttria nanoparticles (Tm:Y_2O_3) with mean particle size (d_{50}) less than 150 nm in aqueous medium was evaluated. Low concentrated Tm:Y_2O_3 suspensions prepared with 0.05 vol.% solids exhibited variation of isoelectric point (IEP) as a function of thulium concentration (0–2 at%, atomic percentage) from

pH 8.6 to pH 9.2, respectively. Most suspensions presented high stability at pH 10.5 with zeta potential values around - 30 mV. This work innovates by reporting very useful parameters to advance toward new materials for radiation dosimetry.

CRediT authorship contribution statement

S.C. Santos: Conceptualization, Methodology, , Writing - original draft, Writing - review & editing. **O. Rodrigues:** Data curation, Resources, Supervision, Project administration. **L.L Campos:** Data curation, Resources, Supervision, Project administration, Funding acquisition.

Declaration of Competing Interest

The authors report no declarations of interest.

Acknowledgements

We authors are deeply grateful to Dra. Maria Elisa Chuery Martins Rostelato from Radiation Technology Centre (CTR) localized at Nuclear and Energy Research Institute (IPEN/CNEN-SP, Sao Paulo, Brazil) that kindly allowed us to use zeta potential analyzer, and MSc. Beatriz Ribeiro Nogueira from the same centre that helped me during my first time in using the equipment. In addition to the following sponsor organizations: São Paulo Research Foundation (FAPESP); National Council for Scientific and Technological Development (CNPq); and Coordination for Improvement of High Degree People (CAPES).

Appendix A. Supplementary data

Supplementary material related to this article can be found, in the online version, at doi:https://doi.org/10.1016/j.mtcomm.2020.101749.

References

[1] W. Rühm, E. Ainsbury, B. Breustedt, M. Caresana, P. Gilvin, Ž. Knežević, H. Rabus, L. Stolarczyk, A. Vargas, J.F. Bottollier-Depois, R. Harrison, M.A. Lopez, H. Stadtmann, R. Tanner, F. Vanhavere, C. Woda, I. Clairand, E. Fantuzzi, P. Fattibene, O. Hupe, P. Olko, V. Olšovcová, H. Schuhmacher, J.G. Alves, S. Miljanic, The European radiation dosimetry group – Review of recent scientific achievements, Radiat. Phys. Chem. 168 (2020), https://doi.org/10.1016/j.radphyschem.2019.108514, 108514.

[2] B. Aksakal, M. Demirel, The effect of Zirconia/Yttria/Silver substitutions on mechanostructure and cell viability of the synthesized bioceramic bone grafts, Ceram. Int. 43 (2017) 7482–7487, https://doi.org/10.1016/j.ceramint.2017.03.026.

[3] S.C. Santos, C. Yamagata, L.L. Campos, S.R.H. Mello-Castanho, Processing, microstructure and thermoluminescence response of biomorphic yttrium oxide ceramics, Ceram. Int. (2016), https://doi.org/10.1016/j.ceramint.2016.05.136.

[4] M.A. Yar, S. Wahlberg, M.O. Abuelnaga, M. Johnsson, M. Muhammed, Processing and sintering of yttrium-doped tungsten oxide nanopowders to tungsten-based composites, J. Mater. Sci. 49 (2014) 5703–5713, https://doi.org/10.1007/s10853-014-8289-x.

[5] S. Khanmohammadi, E. Taheri-Nassaj, Micro-porous silica-yttria membrane by sol-gel method: preparation and characterization, Ceram. Int. 40 (2014) 9403–9411, https://doi.org/10.1016/j.ceramint.2014.02.010.

[6] F. Hayashi, M. Tanaka, D.M. Lin, M. Iwamoto, Surface structure of yttrium-modified ceria catalysts and reaction pathways from ethanol to propene, J. Catal. 316 (2014) 112–120, https://doi.org/10.1016/j.jcat.2014.04.017.

[7] S. Abubakar, S. Kaya, H. Karacali, E. Yilmaz, The gamma irradiation responses of yttrium oxide capacitors and first assessment usage in radiation sensors, Sensors Actuators A Phys. 258 (2017) 44–48, https://doi.org/10.1016/j.sna.2017.02.022.

[8] D. Ghosh, S. Mukherjee, S. Das, High temperature oxidation behaviour of yttria (Y2O3) coated low alloy steel, Surf. Eng. 30 (2014) 524–528, https://doi.org/10.1179/1743294414y.0000000271.

[9] S.F. Hassan, K.S. Tun, M. Gupta, Effect of sintering techniques on the microstructure and tensile properties of nano-yttria particulates reinforced magnesium nanocomposites, J. Alloys. Compd. 509 (2011) 4341–4347, https://doi.org/10.1016/j.jallcom.2011.01.064.

[10] M. Cesaria, J. Collins, B. Di Bartolo, On the efficient warm white-light emission from nano-sized Y2O3, J. Lumin. 169 (2016) 574–580, https://doi.org/10.1016/j.jlumin.2015.08.017.

[11] A. Govindasamy, C. Lv, H. Tsuboi, M. Koyama, A. Endou, M. Kubo, E. Broclawik, A. Miyamoto, A theoretical study of the effect of Eu ion dopant on the electronic excitations of yttrium oxide and yttrium oxy-sulphide, Japanese J. Appl. Phys. Part 1-Regular Pap. Br. Commun. Rev. Pap. 45 (2006) 5782–5785, https://doi.org/10.1143/Jjap.45.5782.

[12] Y.N. Xu, Z.Q. Gu, W.Y. Ching, Electronic, structural, and optical properties of crystalline yttria, Phys. Rev. B 56 (1997) 14993–15000, https://doi.org/10.1103/PhysRevB.56.14993.

[13] S. Santos, O. Rodrigues, L. Campos, A Glance on Rare Earth Oxides : Importance, Reserves, Demand, Applications, Critical Uncertainties, Global Economy, and Zeta Potential Characterization, 2020, https://doi.org/10.2174/2405465805999200628095450, 1–22.

[14] N.L. Wang, X.Y. Zhang, Z.H. Bai, Synthesis of neodymium doped yttria nanopowders by microwave-assisted glycine combustion method and the powder characteristics, Ceram. Int. 40 (2014) 4903–4908, https://doi.org/DOI 10.1016/j.ceramint.2013.10.073.

[15] H.K. Jung, C.H. Kim, A.-R. Hong, S.H. Lee, T.C. Kim, H.S. Jang, D.H. Kim, Luminescent and magnetic properties of cerium-doped yttrium aluminum garnet and yttrium iron garnet composites, Ceram. Int. 45 (2019) 9846–9851, https://doi.org/https://doi.org/10.1016/j.ceramint.2019.02.023.

[16] E.F. Huerta, J. De Anda, I. Martínez-Merlin, U. Caldiño, C. Falcony, Near-infrared luminescence spectroscopy in yttrium oxide phosphor activated with Er3+, Li+ and Yb3+ ions for application in photovoltaic systems, J. Lumin. 224 (2020), 117271. https://doi.org/https://doi.org/10.1016/j.jlumin.2020.117271.

[17] L. Mariscal-Becerra, V.M. Velázquez-Aguilar, M.C. Flores-Jiménez, J. M. Hernández-Álcantara, E. Camarillo-García, C.J. Villagómez, R. Váquez-Arreguín, I. Martínez-Merlin, C. Falcony-Guajardo, H. Murrieta, Up-conversion luminescence of hafnium, erbium, ytterbium and lithium co-doped yttrium oxide, Opt. Mater. (Amst). 105 (2020), https://doi.org/10.1016/j.optmat.2020.109923, 109923.

[18] J.H.S.K. Monteiro, A. de Bettencourt-Dias, 3 - lanthanide ion emission in multicolor OLEDs (Ce3+, Pr3+, Tb3+, Dy3+, Tm3+, and white light Eu3+/Tb3+ hybrid systems) and device characterization, in: P. Martín-Ramos, M.B.T.-L.-B.M.M. Ramos Silva (Eds.), Adv. Nanomater, Elsevier, 2018, pp. 99–131, https://doi.org/10.1016/B978-0-12-813840-3.00003-X.

[19] X. Jin, M. Zhang, Chapter 3 - 2D materials for laser applications, in: Q. Bao (Ed.), H.Y.B.T.-2D M. for P. and O.A. Hoh, Woodhead Publ. Ser. Electron. Opt. Mater., Woodhead Publishing, 2020, pp. 79–103, https://doi.org/10.1016/B978-0-08-102637-3.00003-6.

[20] L.R.P. Kassab, D.M. da Silva, 12 - Pedestal Doped Waveguides for Infrared Light Amplification, in: L.R.P. Kassab, C.B.B.T.-M.N. for P. de Araujo (Eds.), Nanophotonics, Elsevier, 2019: pp. 303–326. https://doi.org/https://doi.org/10.1016/B978-0-08-102378-5.00012-X.

[21] Y. Gandhi, M.V.R. Rao, C.S. Rao, I.V. Kityk, N. Veeraiah, Role of Al2O3 in upconversion and NIR emission in Tm3+ and Er3+ codoped calcium fluoro phosphorous silicate glass system, J. Lumin. 131 (2011) 1443–1452, https://doi.org/10.1016/j.jlumin.2011.03.046.

[22] M.K. Abd-Rahman, N.I. Razaki, Effect of nanofiber/thin-film multilayers on the optical properties of thulium-doped silica-alumina, J. Lumin. 196 (2018) 442–448, https://doi.org/10.1016/j.jlumin.2018.01.003.

[23] S.C. Santos, W. Acchar, C. Yamagata, S. Mello-Castanho, Yttria nettings by colloidal processing, J. Eur, Ceram. Soc. 34 (2014) 2509–2517, https://doi.org/10.1016/j.jeurceramsoc.2014.03.006.

[24] S. Cardoso Santos, O. Rodrigues, L. Lucente Campos, Advances in colloidal processing of rare earth particles, Curr. Smart Mater. 02 (2017), https://doi.org/10.2174/2405465802666171012143956.

[25] S.C. Santos, O. Rodrigues, L.L. Campos, EPR dosimetry of yttria micro rods, J. Alloys. Compd. (2018), https://doi.org/10.1016/j.jallcom.2018.01.315.

[26] S.C. Santos, O. Rodrigues, L.L. Campos, EPR response of yttria micro rods activated by europium, J. Alloys. Compd. (2018), https://doi.org/10.1016/j.jallcom.2018.06.063.

[27] S.C. Santos, O. Rodrigues, L.L. Campos, Bio-prototyping of europium-yttria based rods for radiation dosimetry, Mater. Chem. Phys. (2017), https://doi.org/10.1016/j.matchemphys.2017.07.063.

[28] A.L. Patterson, The Scherrer formula for x-ray particle size determination, Phys. Rev. 56 (1939) 978–982, https://doi.org/10.1103/Physrev.56.978.

[29] W. Tscharnuter, Photon Correlation Spectroscopy in Particle Sizing, 1st ed., John Wiley & Sons Ltd, United States of America, 2000. http://www.brookhaveninstruments.com/literature/lit_90Plus.html.

[30] D.N. Thomas, S.J. Judd, N. Fawcett, Flocculation modelling: a review, Water Res. 33 (1999) 1579–1592, https://doi.org/10.1016/S0043-1354(98)00392-3.

[31] R. Moreno, Reología de suspensiones cerámicas. Consejo Superior De Investigaciones Científicas, Spain, 1st ed., 2005.

[32] L. Meites, P. Zuman, H.W. Nurnberg, Recommended terms, symbols, and definitions for electroanalytical chemistry (Recommendations 1985), Pure Appl. Chem. 57 (1985) 1491, https://doi.org/10.1351/pac198557101491.

[33] J.C. Slater, Atomic radii in crystals, J. Chem. Phys. 41 (1964) 3199–3204, https://doi.org/10.1063/1.1725697.

[34] D.V. Tolstikova, M.D. Mikhailov, V.M. Smirnov, Features of the synthesis of nanoparticles of yttrium oxide Y2O3:Nd, Russ. J. Gen. Chem. 84 (2014) 2043–2044, https://doi.org/10.1134/S1070363214100314.

[35] V. Lojpur, S.P. Ahrenkiel, M.D. Dramicanin, Yb3+, Er3+ doped Y2O3 nanoparticles of different shapes prepared by self-propagating room temperature reaction method, Ceram. Int. 40 (2014) 16033–16039, https://doi.org/10.1016/j.ceramint.2014.07.139.

[36] M. Foex, Allotropic transformations of rare earth sesquioxides, J. Inorg. Gen. Chem. ZAAC. 337 (1965) 313–324, https://doi.org/10.1002/zaac.19653370511.
[37] P. Aldebert, J.P. Traverse, Neutron diffraction study of high temperature structures of La2O3 and Nd2O3, Mater. Res. Bull. 14 (1979) 303–323, https://doi.org/10.1016/0025-5408(79)90095-3.
[38] G. Brauer, Progress in the Science and Technology of the Rare Earths, Pergamon Press, Oxford, 1966. https://scholar.google.com/scholar_lookup?hl=en&publication_year=1966&pages=312&author=G.+Brauer&title=Progress+in+the+Science+and+Technology+of+the+Rare+Earths.
[39] J.J. Ryszard, Sprycha Egon Matijevic, zeta potential and surface charge of monodispersed colloidal yttrium (III) oxide and basic carbonate, J. Colloid Interface Sci. 149 (1991) 562–568, https://doi.org/10.1016/0021-9797(92)90443-P.
[40] I. ulHaq, E. Matijevic, Preparation and properties of uniform coated inorganic colloidal particles .10. Manganese compounds on hematite, J. Colloid Interface Sci. 192 (1997) 104–113, https://doi.org/10.1006/jcis.1997.5002.
[41] C. del Angel-Olarte, L. Hernández-Adame, A. Mendez-Blas, G. Palestino, Eu3+/Yb3+ co-doped gadolinium oxysulfide upconverting nanorods: morphological, physicochemical and optical evaluation, J. Alloys. Compd. 787 (2019) 1032–1043, https://doi.org/10.1016/j.jallcom.2019.02.113.
[42] L. Liu, Y. Wang, S. Craik, W. James, Z. Shu, R. Narain, Y. Liu, Removal of Cryptosporidium surrogates in drinking water direct filtration, Colloids Surf. B Biointerfaces 181 (2019) 499–505, https://doi.org/10.1016/j.colsurfb.2019.05.065.
[43] S.C. Santos, L.F.G. Setz, C. Yamagata, S.R.H. Mello-Castanho, Rheological Study of Yttrium Oxide Aqueous Suspensions, 2010, https://doi.org/10.4028/www.scientific.net/MSF.660-661.712.
[44] S.C. Santos, C. Yamagata, L.L. Campos, S.R.H. Mello-Castanho, Bio-prototyping and thermoluminescence response of cellular rare earth ceramics, J. Eur. Ceram. Soc. 36 (2016) 791–796, https://doi.org/10.1016/j.jeurceramsoc.2015.10.024.
[45] S.C. Santos, C. Yamagata, A.C. Silva, L.F.G. Setz, S.R.H. Mello-Castanho, Yttrium disilicate micro-cellular architecture from biotemplating of Luffa Cylindrica, J. Ceram. Sci. Technol. 5 (2014) 203–208, https://doi.org/10.4416/JCST2014-00008.
[46] S.C. Santos, C. Yamagata, L.L. Campos, S.R.H. Mello-Castanho, Processing and thermoluminescent response of porous biomorphic dysprosium doped yttrium disilicate burner, Mater. Chem. Phys. 177 (2016) 505–511, https://doi.org/10.1016/j.matchemphys.2016.04.061.
[47] G. Xia, S. Zhou, J. Zhang, J. Xu, Structural and optical properties of YAG:Ce3+ phosphors by sol–gel combustion method, J. Cryst. Growth 279 (2005) 357–362, https://doi.org/10.1016/j.jcrysgro.2005.01.072.
[48] H.M.H. Fadlalla, C.C. Tang, YAG:Ce3+ nano-sized particles prepared by precipitation technique, Mater. Chem. Phys. 114 (2009) 99–102, https://doi.org/10.1016/j.matchemphys.2008.08.049.